Journal of Power Sources 196 (2011) 1776–1794

Contents lists available at ScienceDirect

Journal of Power Sources

journal homepage: www.elsevier.com/locate/jpowsour

Liquid water flooding process in proton exchange membrane fuel cell cathode with straight parallel channels and porous layer

Xichen Wang, Biao Zhou*

Department of Mechanical, Automotive and Materials Engineering, University of Windsor, 401 Sunset Ave., Windsor, ON, Canada N9B 3P4

ARTICLE INFO

Article history:
Received 8 August 2010
Received in revised form
29 September 2010
Accepted 29 September 2010
Available online 7 October 2010

Keywords:
Proton exchange membrane fuel cell
Parallel
Water management
Volume of fluid

ABSTRACT

Liquid water management plays a significant role in proton exchange membrane fuel cell (PEMFC) performance, especially when the PEMFC is operating with high current density. Therefore, understanding of liquid water behavior and flooding process is a critical challenge that must be addressed. To overcome PEMFC durability problems, a liquid water flooding process is studied in the cathode side of a PEMFC with straight parallel channels and a porous layer using FLUENT® v6.3.26 software with a volume-of-fluid (VOF) algorithm and user-defined-function (UDF). The general process of liquid water flooding within this type of PEMFC cathode is investigated by analyzing the behavior of liquid water in porous layer and gas flow channels. Two important phenomena, the "first channel phenomenon" and the "last channel phenomenon", and their effects on the flow distribution along different parallel channels are discussed.

1. Introduction

A fuel cell is an environment friendly energy conversion device that directly converts chemical energy into electrical energy. It is regarded as a major alternative to traditional energy sources such as internal combustion engines. Due to the advantages of its low operating temperature and high power density, proton exchange membrane fuel cell (PEMFC) is considered one of the potential candidates for commercialization.

For the last two decades, although many different types of PEMFC flow-field designs have been developed by industrial and academic researchers [1], most of them can be classified into parallel, serpentine, or interdigitated category [2]. These different designs were proposed to resolve the major concerns, such as pressure drop, uniformity of reactant gas distribution, and liquid water management.

As a critical research topic for optimizing the performance of PEMFCs, liquid water management is attracting great efforts from many scientists and engineers [3].

Djilali et al. [4] developed a two-dimensional model to investigate the transport process in PEMFCs to improve water management. Previously reported analyses by Djilali and Lu [5] also studied the influence of heat and water transport in PEMFCs. A three-dimensional numerical model of straight gas-flow channels was studied by Dutta et al. [6] using the commercial computational fluid dynamics (CFD) software FLUENT®. Cha et al. [7] discussed the influence of oxygen concentration along gas flow channels on PEMFC performance by examining the steady-state gas-flow phenomena in micro parallel flow channels. Kulikovsky [8] numerically acquired the gas concentration of a steady-state flow along channels in a similar way. These studies, however, did not investigate the influence of liquid water. Yi et al. [9] indicated that water vapor condensation is a common phenomenon on both sides of a PEMFC. You and Liu [10] pointed out that a multi-phase model must be employed in order to obtain more practical results. Both of these previous studies considered water in vapor form [9,10]. Wang et al. conducted a two-phase, multi-component mixture model of the cathode of a PEMFC to deal with the problems in a single- and in a two-phase co-existence region [11] and introduced a technique to measure in situ water distribution [12]. Recently, Dawes et al. [13] investigated the effects of water with a three-dimensional mixture model of a PEMFC, and Wang et al. also developed a topologically equivalent pore network model to study the transport of liquid water in PEMFC [14].

Zhou et al. made significant efforts in investigating liquid water behavior in PEMFCs, including in single cells and in stacks. Volume-of-fluid (VOF) model was applied to simulate the process of liquid water removal using FLUENT® [15]. Zhou et al. also conducted a numerical simulation of two-phase flow in several different types of cathode design, e.g., in stack with parallel serpentine channels [16] and in stack with straight micro parallel channels [17]. Different innovative gas diffusion layers (GDL), their water removal characteristics [18], the effects of electrode wettability on liquid water behavior [19], and accelerated numerical test of liquid behavior

* Corresponding author. Tel.: +1 519 253 3000x2630; fax: +1 519 973 7007.
E-mail address: bzhou@uwindsor.ca (B. Zhou).

0378-7753/$ – see front matter © 2010 Elsevier B.V. All rights reserved.
doi:10.1016/j.jpowsour.2010.09.092

Nomenclature

s	momentum source term
g	acceleration of gravity ($m\,s^{-2}$)
$\boldsymbol{u}$	velocity vector ($m\,s^{-1}$)
K	surface curvature
s	phase volume fraction
ρ	density
ε	porosity
μ	dynamic viscosity (Pa s)
χ	surface tension coefficient
α	gaseous permeability (m^2)

Subscripts

g	gas
l	liquid
c	continuity equation
m	momentum equation

across GDL [20] were investigated using the VOF method. Djilali et al. [21] also used the VOF method to study the dynamic behavior of liquid water emerging from a GDL pore into a PEMFC gas-flow channel. Several reports have contributed to the fundamental understanding of liquid water behavior inside flow channels [16–19], but conventional porous layers were not included in these analyses. Electro-chemical reactions have also been neglected.

A general model for PEMFCs [22] has been proposed and applied to investigate two-phase flow coupled with electro-chemical reactions, water transport through the membrane and heat and mass transfer for single cells with serpentine channels [22], single cells with serpentine-parallel channels [23], and 3-cell stack with parallel design [24]. These previous studies [22–24] are the state of the art for simulating PEMFCs; however, this technique requires excessive computational time.

Recently, Zhou et al. [25] conducted numerical simulation of liquid water behavior in cathode of a PEMFC with serpentine channels and porous layer, using a simplified model in which electro-chemical reactions and heat transfer effects were neglected to minimize the computation time. Also detailed experimental validation of this simplified cathode model was performed by direct optical visualization method to capture the motion and deformation of liquid water with high spatial and temporal resolutions. For

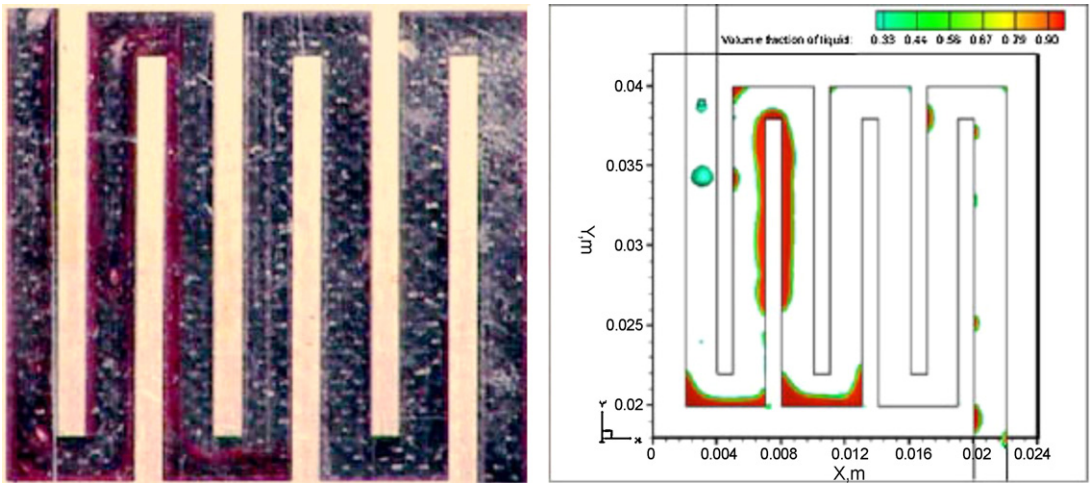

Fig. 1. Comparison of liquid water behaviors between numerical simulation and the experiment at $t = 0.400$ s (the left panel shows the experimental setup, and the right panel shows the numerical simulation).

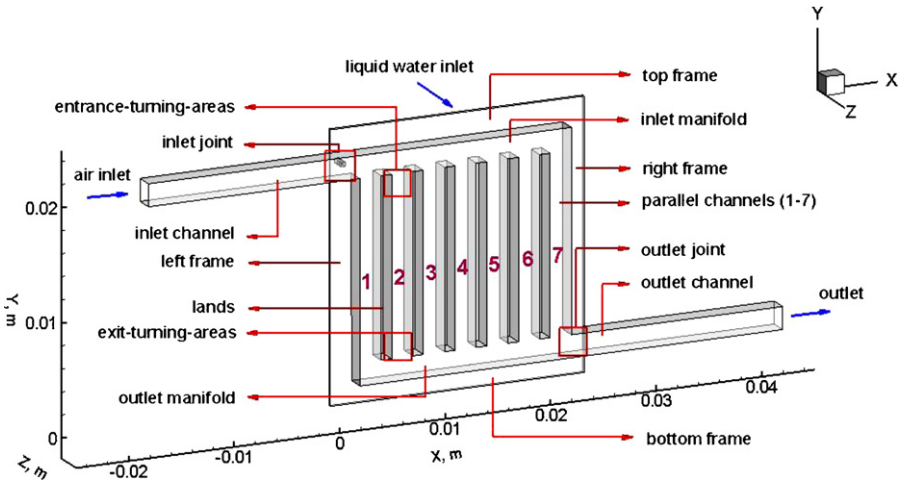

Fig. 2. Simulation domain.

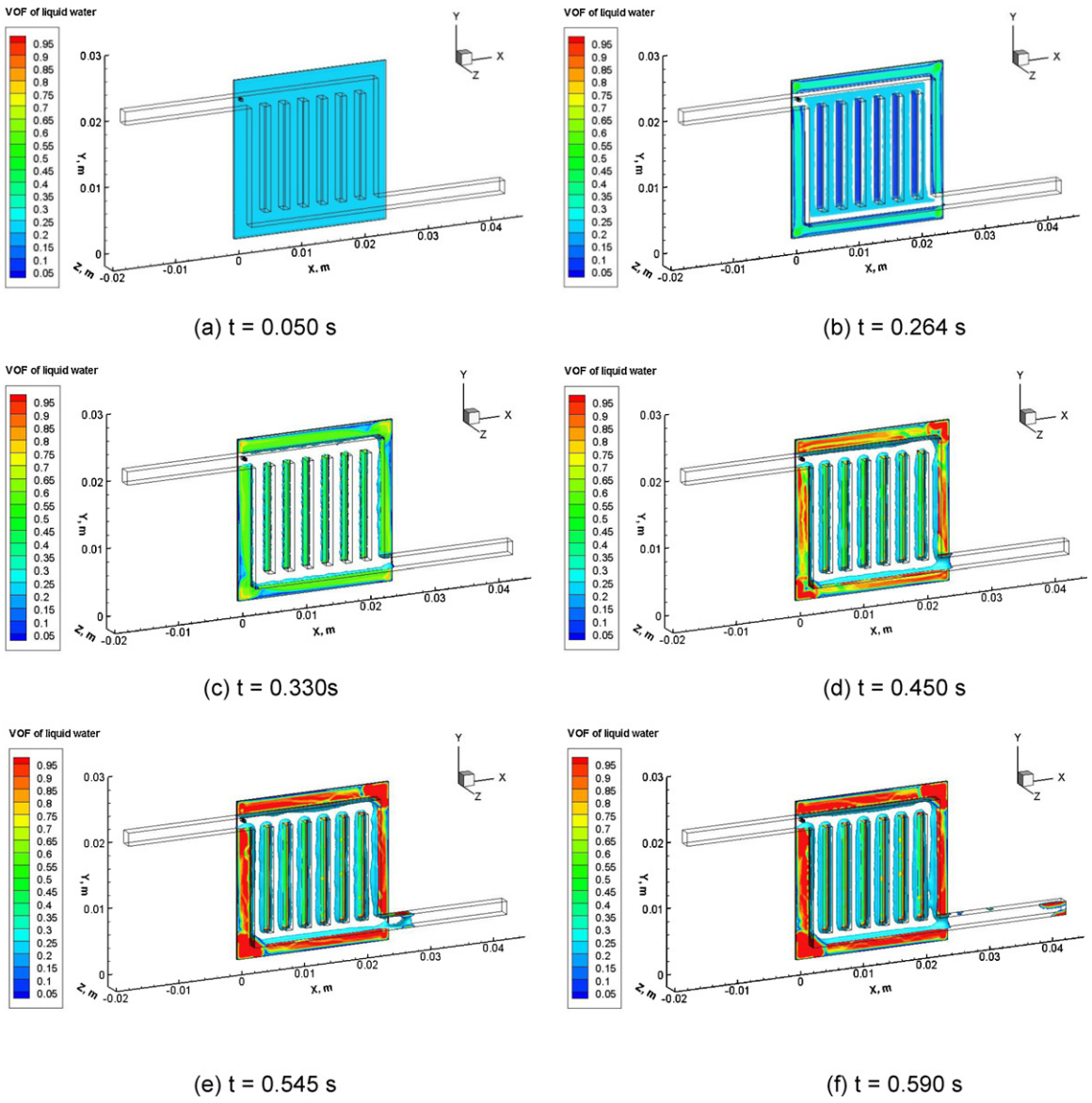

Fig. 3. (a–f) General process of liquid water removal: (a) $t = 0.050$ s; (b) $t = 0.264$ s; (c) $t = 0.330$ s; (d) $t = 0.450$ s; (e) $t = 0.545$ s; (f) $t = 0.590$ s.

reader's convenience, a sample comparison from this validation is shown in Fig. 1, which demonstrates that the results from this simplified model are in good agreement with the corresponding experiments.

From above literature review, some key points could be summarized as follows:

(1) Although significant efforts have been made to understand the liquid water effects on PEMFC, the liquid water flooding process still remain to be investigated for all kinds of flow field designs. For example, PEMFC with parallel channel design suffers from liquid water flooding, while there is no literature available to address this important issue with VOF method.
(2) The VOF method with serpentine PEMFC application has been validated by experiments [25] and it can be employed in the investigation of PEMFC with other different types of flow field designs.
(3) There are three different ways to introduce liquid water in VOF modeling of PEMFC: presetting certain amounts of droplets [15–17,22,23,25] or certain liquid water film(s) [16,17], injecting liquid water droplets through a pinhole [21,24], and setting liquid water flowrate using the accelerated numerical method [20]. The third one can provide significant insights into the fundamental understanding of liquid water flooding process inside PEMFC with an acceptable computation time.

Using the numerical methodology developed and validated in the present authors' previous works [20,25] as an engineering research tool, the present paper investigates the liquid water behavior inside a PEMFC cathode with straight parallel channels and a porous layer to gain the fundamental understanding on the liquid water flooding process within this type of PEMFC design.

In the following sections, the numerical simulation domain, mathematical model, mesh independency, and initial settings are introduced. These sections are followed by a detailed discussion of liquid water flooding process, porosity effects on drainage performance, and conclusions.

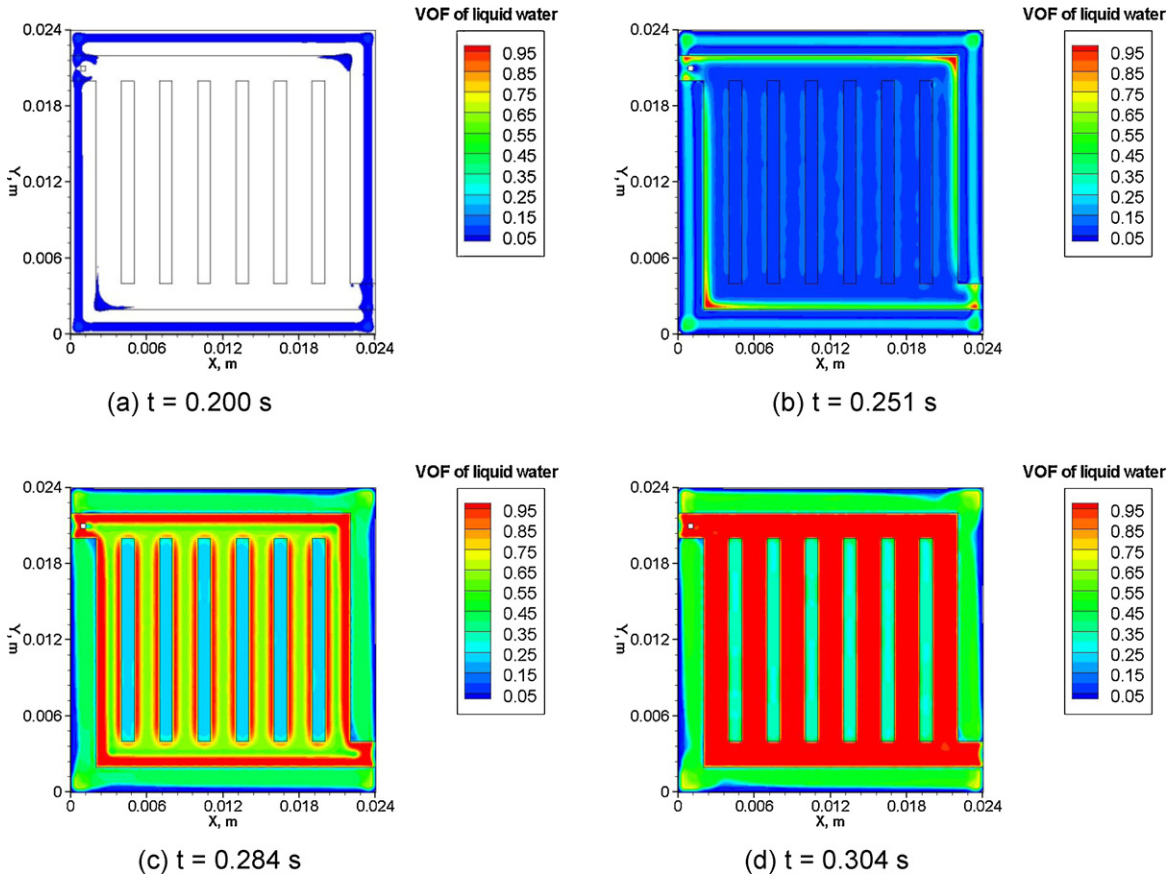

Fig. 4. (a–d) Liquid water distribution at $Z = 0.00029$ m: (a) $t = 0.200$ s; (b) $t = 0.251$ s; (c) $t = 0.284$ s; (d) $t = 0.304$ s.

2. Numerical model setup

2.1. Numerical simulation domain and boundary conditions

The numerical simulation domain represents as full-scale cathode side geometry of a single PEMFC. Fig. 2 illustrates the schematic of the numerical simulation domain, which contains gas flow channels and a porous layer. The channels are in a parallel pattern, which permits a low overall pressure drop between the gas inlet and the outlet. There are seven parallel channels, with a 0.001 m distance between adjacent channels. The length of the cathode from the air inlet to the outlet is 0.06 m in the *X*-direction. The width of the gas flow channel domain is 0.02 m in the *Y*-direction. The cross-section of the channels is 0.002 m (in the *X*-direction) × 0.002 m (in the *Y*-direction) × 0.0017 m (in the *Z*-direction). The dimensions of the porous layer are 0.024 m (in the *X*-direction) × 0.024 m (in the *Y*-direction) × 0.0003 m (in the *Z*-direction); these are the typical dimensions of a fuel cell component. A liquid water injection channel (LWIC) with dimensions of 0.0004 m (in the *X*-direction) × 0.0004 m (in the *Y*-direction) × 0.000725 m (in the

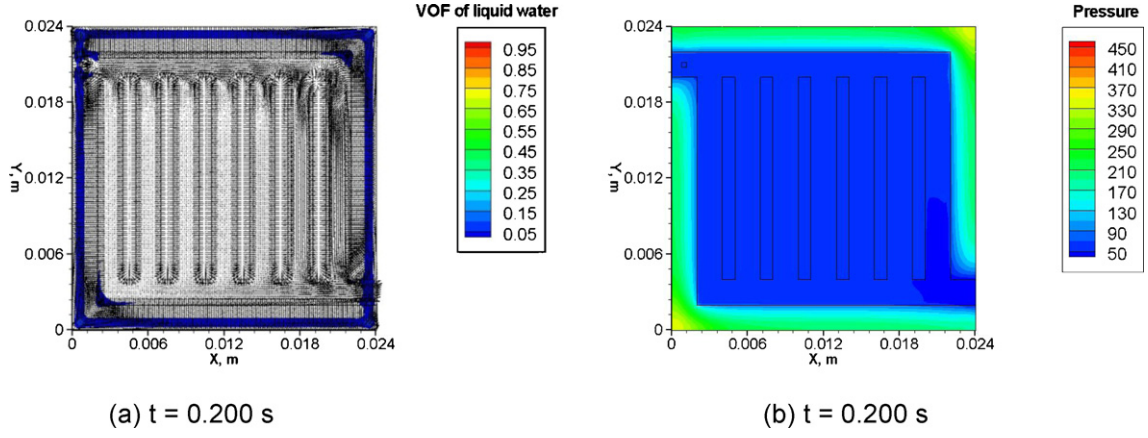

Fig. 5. (a) VOF and velocity distribution at $Z = 0.00029$ m and (b) pressure distribution at $Z = 0.00029$ m. (a) $t = 0.200$ s and (b) $t = 0.200$ s.

Z-direction) is positioned at the inlet joint (defined in Fig. 2). This LWIC was used to simulate liquid water injection effects in previous studies [23] from Zhou's group. In the present study, the LWIC is blocked because there no liquid water is injected through it in this study, and this geometry is kept so that the results for the current study (where the liquid water is supplied from the back surface of the porous layer as shown in Fig. 2) can be compared to the results of previous studies (where liquid–water injection is performed through the LWIC). The direction of gravity is along the negative Z-direction, which is the normal direction of the porous layer, as shown in Fig. 2.

A no-slip boundary condition is applied to the walls. The air inlet is set with a flowrate of 2.00×10^{-5} kg s^{-1} (the flow is normal to the inlet boundary) and the liquid water inlet (back surface of the porous layer shown in Fig. 2) is set with a flowrate of 1.70×10^{-4} kg s^{-1}. The pressure outlet is applied at the outlet boundary. The contact angles, which are set in the side walls of channels, upper walls of channels and the rest of walls, are 40°, 43° and 140°, respectively. The porosities of the porous layers used in this model are 0.3, 0.5 and 0.8 for the three different cases conducted in the present study.

2.2. Computational methodology

The simulation of a three-dimensional, unsteady, two-phase flow, in which the air is treated as gaseous phase and the liquid water is treated as liquid phase (the two phases are assumed to be immiscible in this model), is conducted using FLUENT® v6.3.26 software. The VOF method is applied to track the air–water flow interface inside the computational domain, and the UDF is applied to introduce the source term.

In this model, the fluid flow is laminar because of the low flow velocity and the small size of the channels. In respect that heat transfer and phase change are not considered in this study in order to save the computation time, the unsteady, laminar flow model is governed by the following continuity (mass)

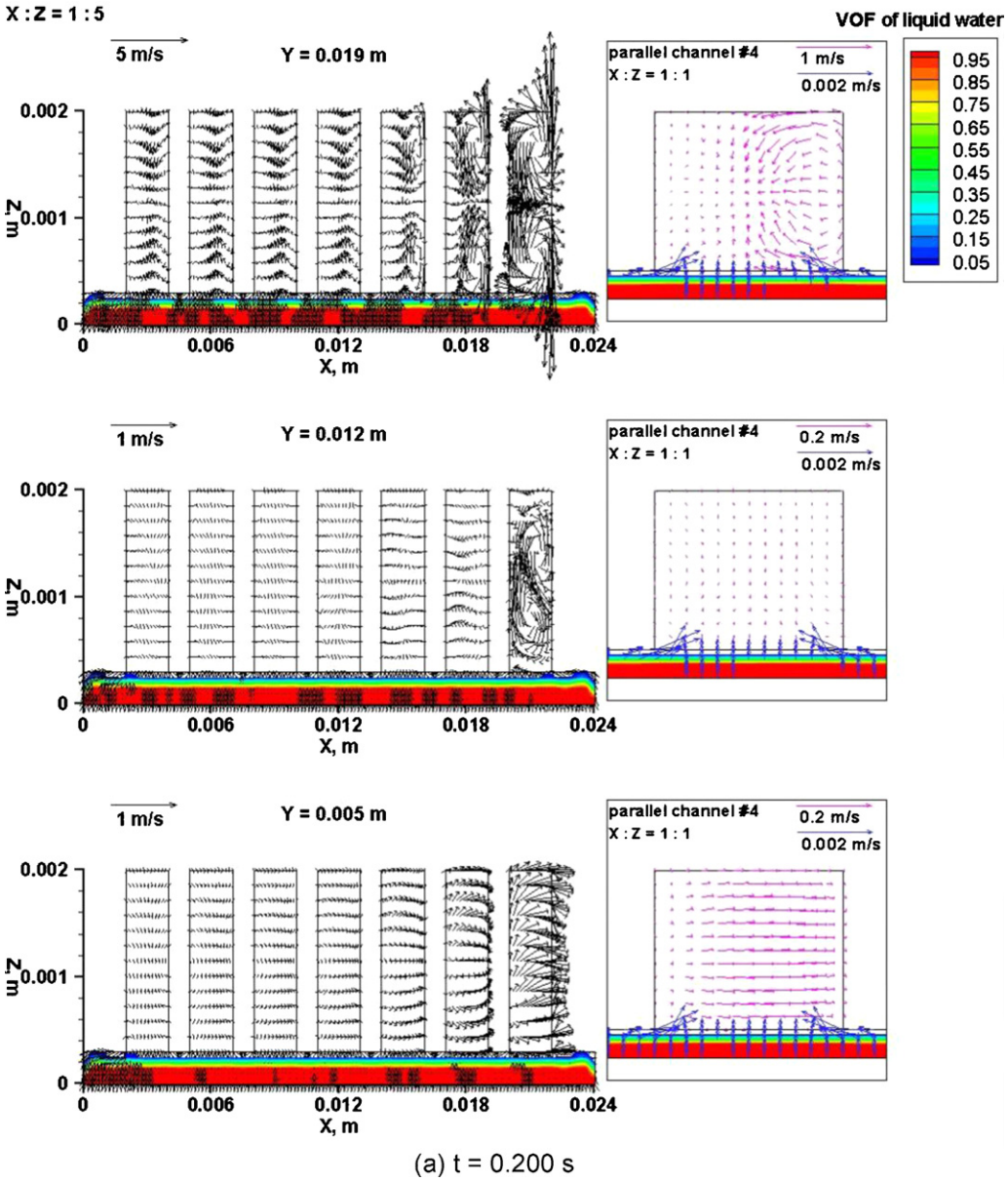

Fig. 6. (a–h) General process by which liquid water emerges into the channels: (a) $t = 0.200$ s; (b) $t = 0.251$ s; (c) $t = 0.284$ s; (d) $t = 0.304$ s; (e) $t = 0.322$ s; (f) $t = 0.388$ s; (g) $t = 0.500$ s; (h) $t = 0.655$ s.

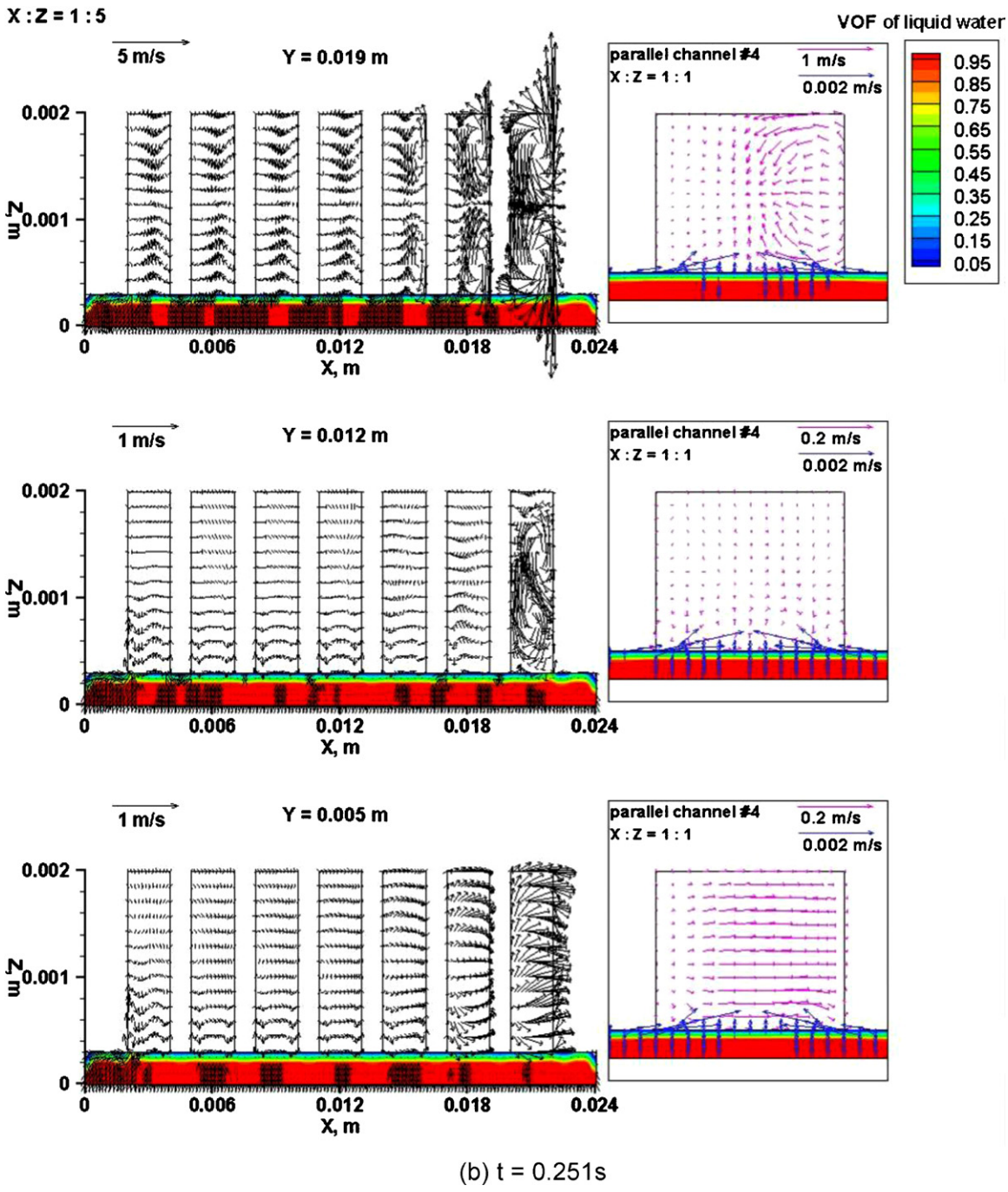

Fig. 6. (*Continued*)

and momentum equations to describe the fluid flow transport process.

The continuity (mass) equation is expressed as

$$\frac{\partial(\varepsilon\rho)}{\partial t} + \nabla\cdot(\varepsilon\rho\boldsymbol{u}) = S_c \tag{1}$$

where ε is the porosity of the porous media (in the gas flow channels $\varepsilon = 1$). The first term on the left hand side is the transient term standing for the change of mass with time, the second term is the convection term standing for the change in mass flux, and the term on the right hand side is the mass source term which equals to zero because phase changes are not taken into account in this model.

In the VOF model, the volume fractions of gas and liquid water are defined as s_l and s_g, respectively, and

$$s_l + s_g = 1 \tag{2}$$

The variables and properties are shared by both phases and are calculated by a volume-averaged method. The average density and viscosity for each computational cell which are between those of gaseous and liquid phases, are defined as

$$\rho = s_l\rho_l + s_g\rho_g \tag{3}$$

and

$$\mu = s_l\mu_l + s_g\mu_g \tag{4}$$

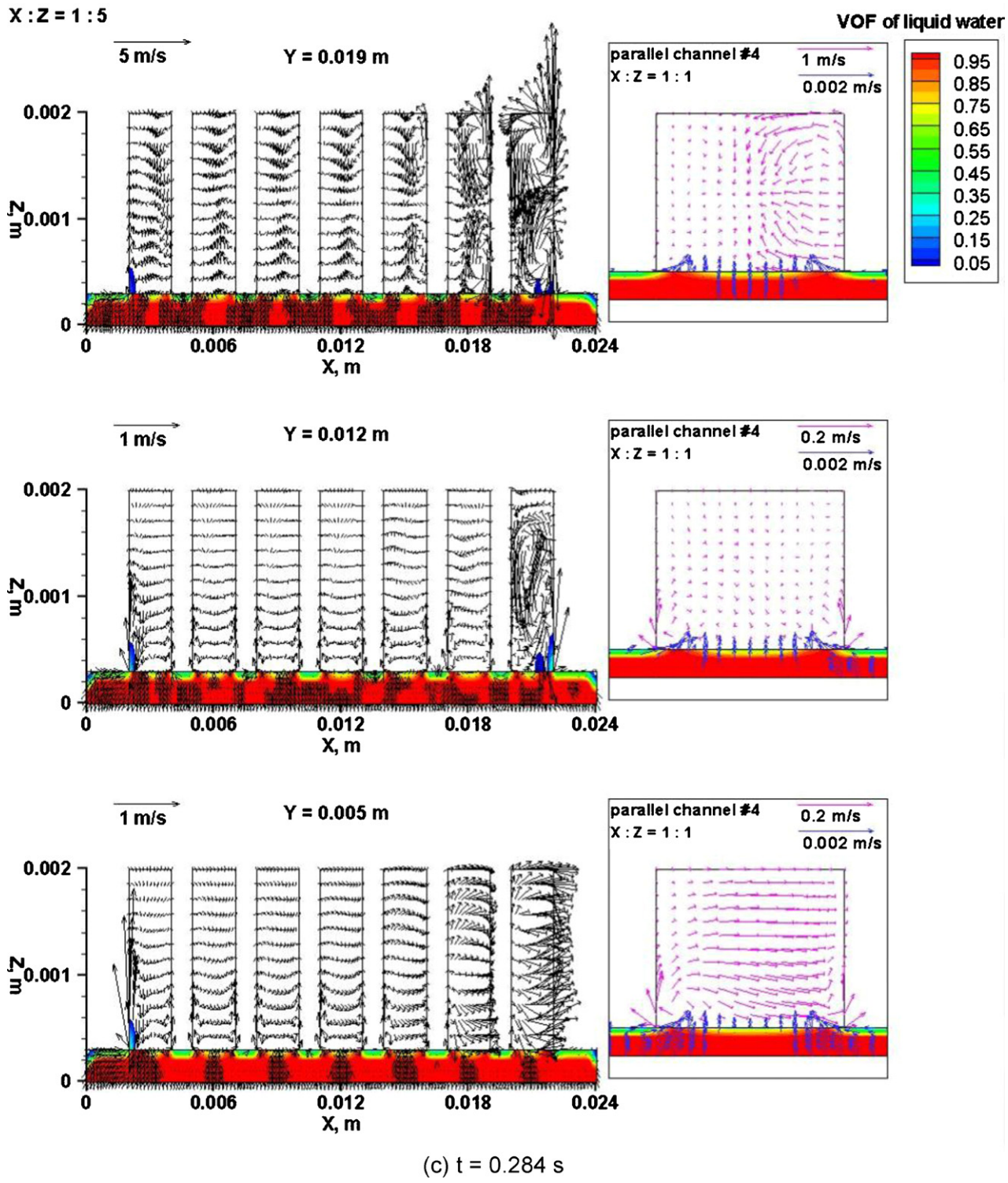

Fig. 6. (*Continued*)

In this VOF model, the interface between gaseous and liquid phases is tracked by solving a continuity equation, i.e., Eq. (5), for the volume fraction of liquid water, which is solved over the entire computational domain. Then the volume fraction of gas is computed based on Eq. (2).

$$\frac{\partial(\varepsilon s_l \rho_l)}{\partial t} + \nabla \cdot (\varepsilon s_l \rho_l \boldsymbol{u}) = 0 \tag{5}$$

The Geo-Reconstruct scheme is applied to smooth the interface between two phases using a piecewise-linear approach, which is more accurate than other methods in FLUENT® [26].

A single momentum equation, i.e., Eq. (6), is implemented in the VOF model, and the gaseous phase and the liquid phase share the same resulting velocity field.

$$\frac{\partial}{\partial t}(\varepsilon \rho \boldsymbol{u}) + \nabla \cdot (\varepsilon \rho \boldsymbol{u}\boldsymbol{u}) = -\varepsilon \nabla p + \nabla[\varepsilon \mu \nabla \boldsymbol{u}] + \varepsilon S_m \tag{6}$$

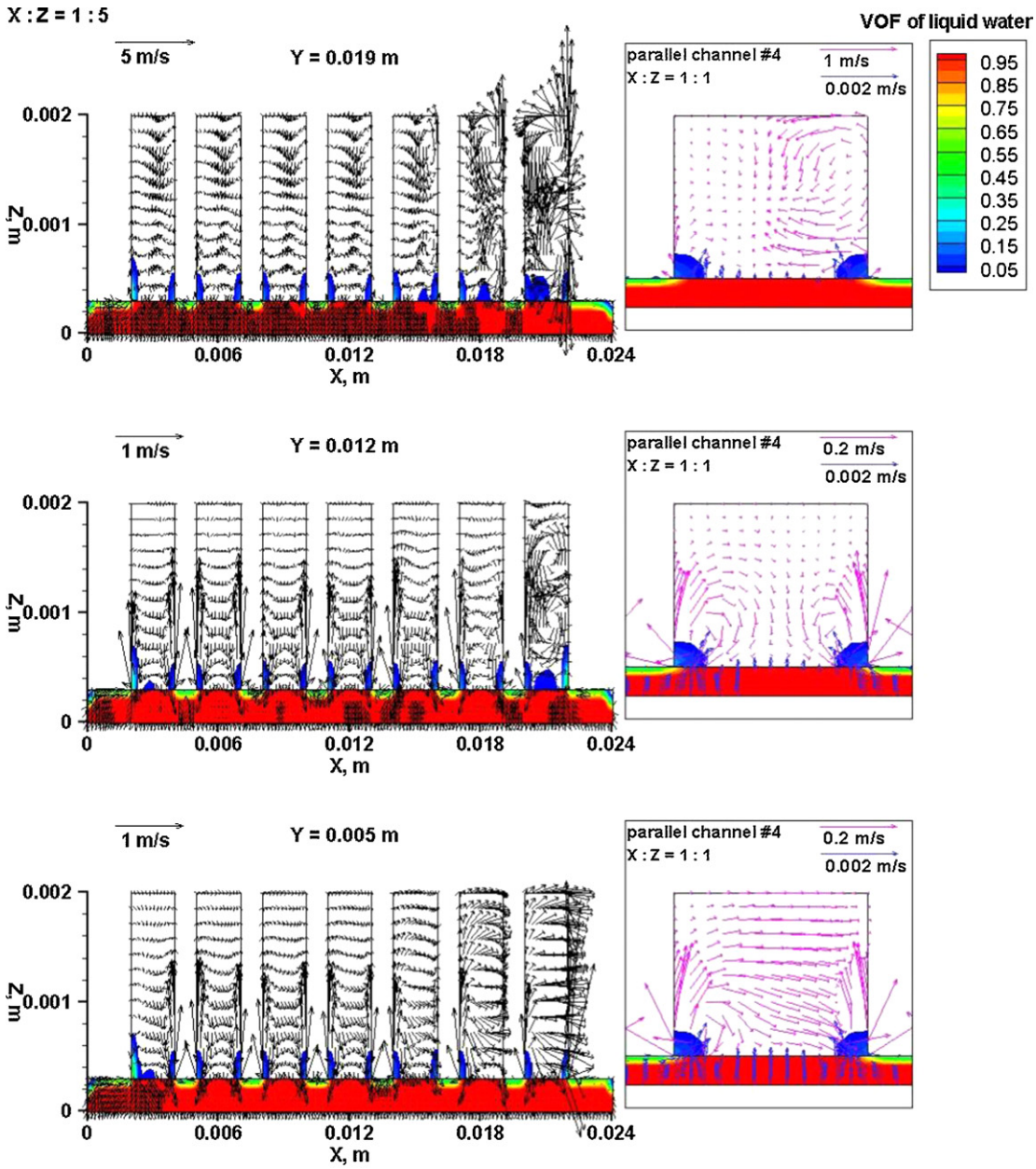

(d) t = 0.304 s

Fig. 6. (*Continued*)

In this momentum equation, the terms on the left hand side represents the change of momentum with time and the advection momentum flux, respectively, while the terms on the right hand side are the momentum due to pressure, viscosity and sources.

In the flow channels of this model, the surface tension force, as well as gravity force, is coupled to the momentum equation by the source term S_m using the continuum surface force (CSF) method [27] which helps smooth the interface in the VOF model, expressed as

$$S_m = \rho_g + \chi K \frac{\rho \nabla s_l}{\rho_l + \rho_g/2} \tag{7}$$

where χ is the surface tension coefficient and K is the curvature.

In the porous layer, one more term $-(\mu/\alpha)\boldsymbol{u}$, where α stands for the permeability of the porous layer, is added in the source term because of the viscous effect though the porous layer, or the Darcy force. So the source term for the momentum equation in the porous layer is

$$S_m = \rho_g + \chi K \frac{\rho \nabla s_l}{\rho_l + \rho_g/2} - \frac{\mu}{\alpha}\boldsymbol{u} \tag{8}$$

2.3. Grid independency

The computation domain is meshed into 290,352 cells with a maximum volume of 5.548611×10^{-12} m^3 and a minimum volume of 5.0×10^{-13} m^3 for each cell. The grid size measures approximately 8.3×10^{-4} m in both the X- and Y-directions, whereas the

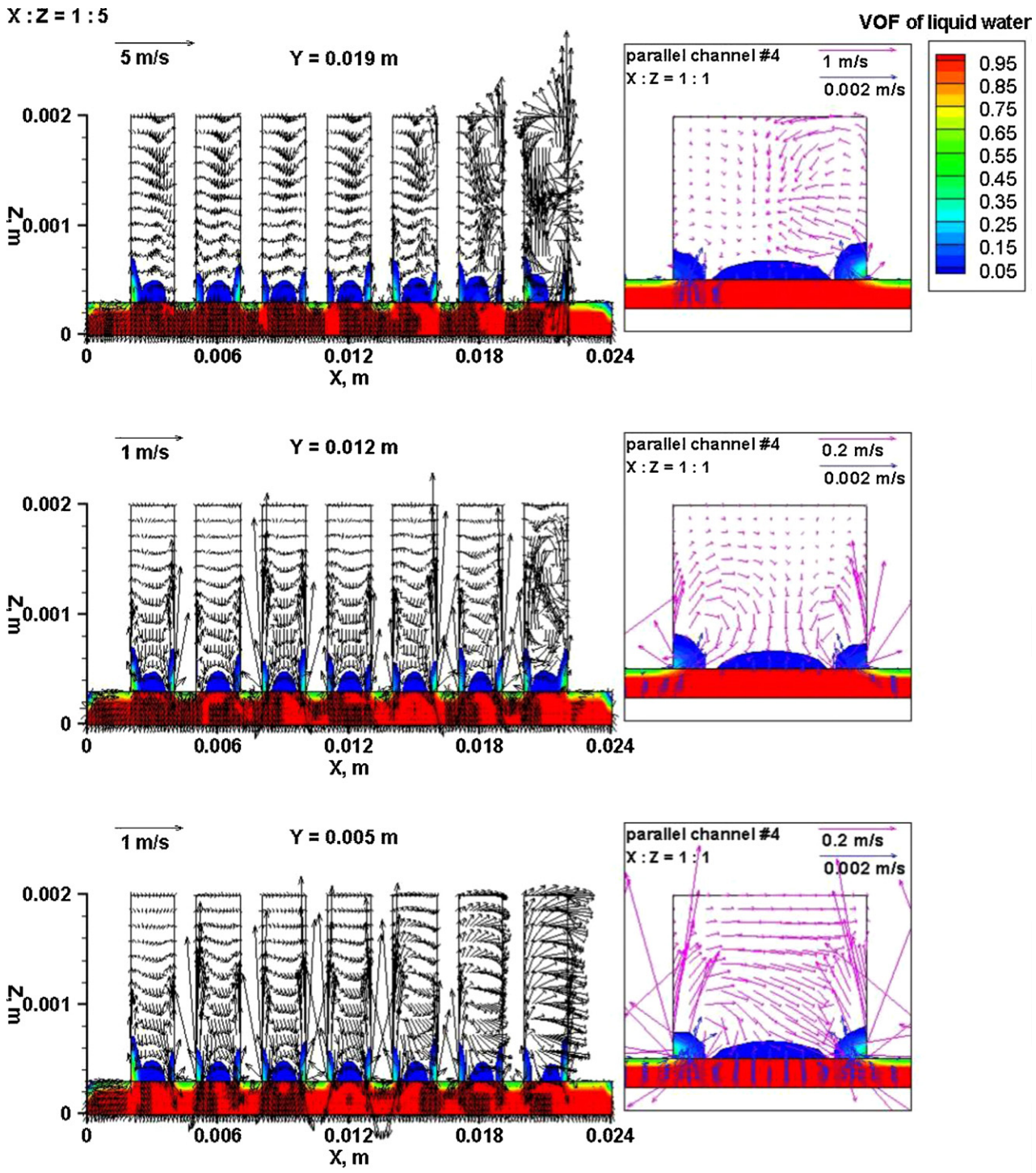

Fig. 6. (*Continued*)

dimensions in the *Z*-direction are 1.4×10^{-4} m in the gas flow channel domain and 5×10^{-5} m in the porous layer domain. Zhou et al. [17] implemented a grid check method by increasing and decreasing the number of grid cells by certain percentages. And this grid size has been validated for PEMFCs by the comparison of numerical results with experimental results from the author's previous studies [25].

3. Results and discussion

In this study, three cases with different porosities (0.3, 0.5 and 0.8) have been investigated. The general water flooding processes between these three cases are quite similar; therefore, in the following sections, the model with a porosity of 0.3 is used for the general discussion. The porosity effect on flooding process is also addressed.

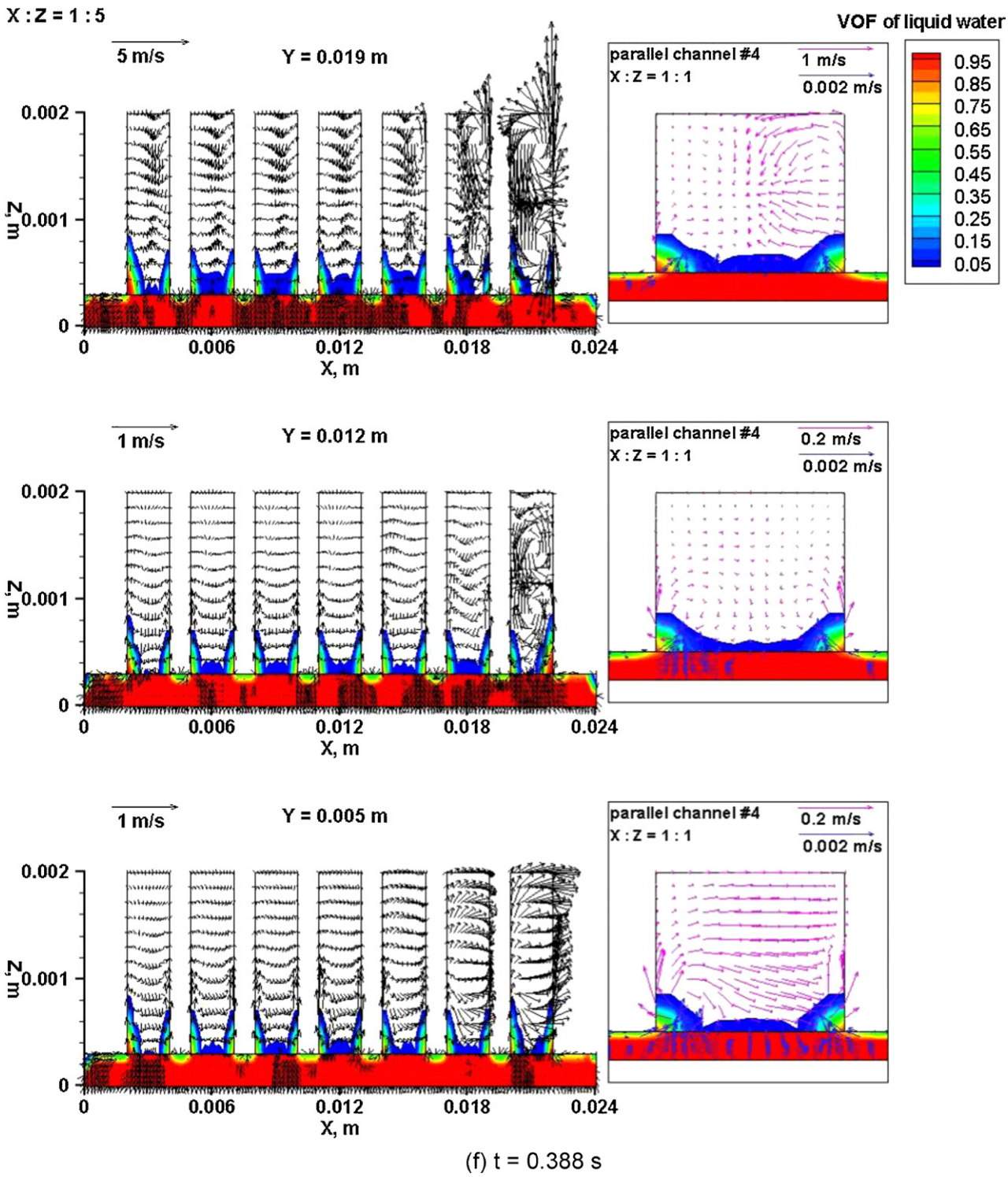

Fig. 6. (*Continued*)

3.1. General process of liquid water removal

Fig. 3(a)–(f) shows the main process of water movement over time for some selected time instants. The general process of liquid water removal can be divided into the following sub-processes:

(1) Liquid water is supplied from the back surface of the porous layer by a constant flowrate to simulate the water generation through electro-chemical reaction (Fig. 3(a)).
(2) This supplied liquid water first enters the porous layer and moves around with in the porous layer (Fig. 3(b)).
(3) Liquid water from the porous layer emerges into gas flow channels from the peripheral edges of lands (solid between adjacent parallel channels defined in Fig. 2) and the peripheral edges of the frames (Fig. 3(c)).
(4) The liquid water emerging into the channels accumulates at the outlet joint (Fig. 3(d)).
(5) The liquid water at outlet joint starts to move into the outlet channel (Fig. 3(e)).

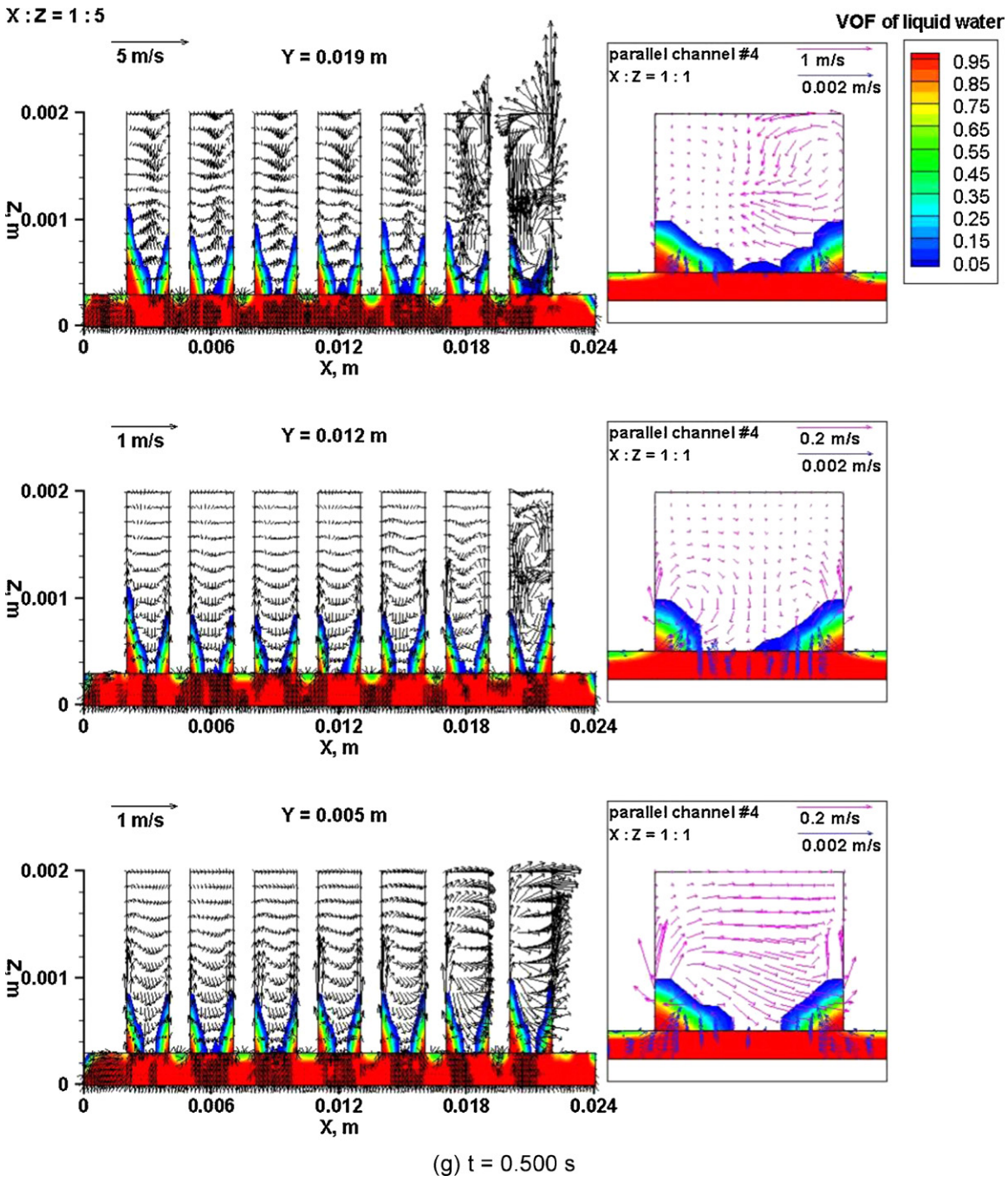

Fig. 6. (*Continued*)

(6) Liquid water drains out through the outlet channel (Fig. 3(f)).

3.2. Liquid water emerging process

3.2.1. Liquid water emerging from the peripheral areas of lands and frames

As shown in Figs. 4(a)–(d) and 5(a) and (b), a plane from the porous layer domain (with projective channel edges) at $Z = 0.00029$ m, which is very close to the interface between porous layer and channels, is extracted to explain the main process of liquid water entering into the channels from the porous layer. Fig. 4(a) shows that the water initially emerges from the outskirts of the porous layer (the porous layer area under the frames) and from the left-bottom and right-top corners of the areas near the flow channels. Fig. 5(a) and (b) gives the velocity and pressure distributions at the same time instant that is used in Fig. 4(a) ($t = 0.200$ s). Fig. 5(a) shows that liquid water accumulates in the outskirts and corners of the porous layer due to the constraint of the porous layer domain, so the pressure in these areas is higher than that in other areas of the porous layer (Fig. 5(b)), resulting in a flow from the outskirt areas to the peripheral edges of the frames (Fig. 5(a)) inside the porous layer. This flow explains why liquid water emerges initially from the peripheral edges of the frames, as shown in Fig. 4(b). Fig. 4(b)–(d) shows that water enters into the channels from the edges of lands (the ribs between two adjacent

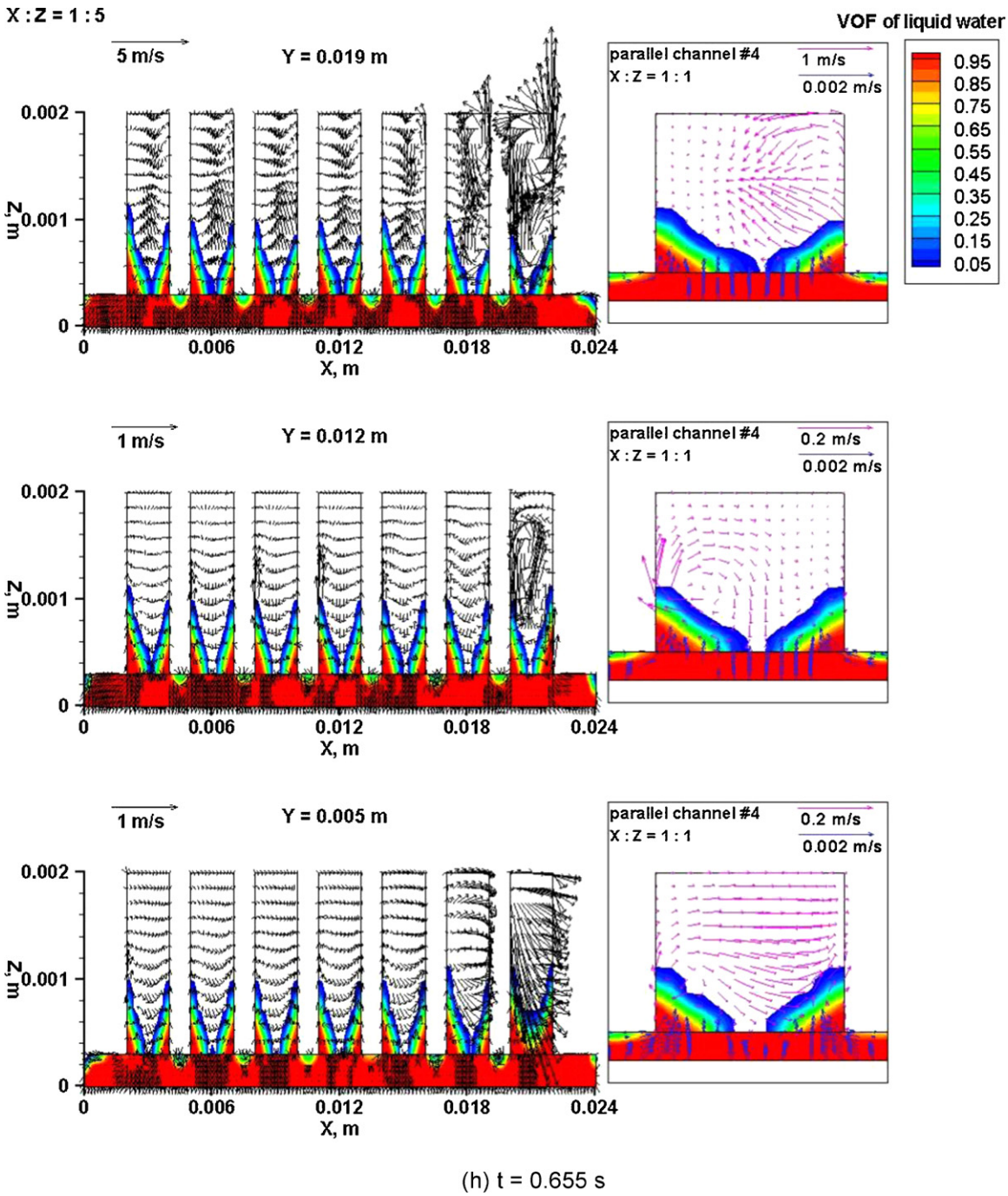

Fig. 6. (*Continued*).

flow channels as defined in Fig. 2) and fills in the areas underneath the channels.

The liquid water emergence from the porous layer into channels can be explained by Fig. 6(a)–(h), which shows the velocity vectors and VOF on the *X*–*Z* planes located at $Y = 0.019$ m, 0.012 m, and 0.005 m with different reference velocity vectors.

The liquid water from the porous layer enters into the channels from the edges of the lands because the liquid water generation rate is uniform on the back surface of the porous layer, but the liquid water underneath the lands cannot directly enter into the channels in the manner that the liquid water underneath the middle of the channels enters. Actually, the liquid water underneath the lands has to detour along the interface between the lands and the porous layer then into the channels (Fig. 6(a)–(d)) because the lands are solid and only allow the conduction of electrons. The liquid water emerges into the channel directly through the porous layer underneath the middle of the channels (Fig. 6(e)), moving with the main gas flow along the parallel channels, and gradually merges with the liquid water that has accumulated around the corners of the channels (Fig. 6(f)–(h)) due to surface tension and wall adhesion effects.

The emergence of liquid water from the porous layer into the channels has direct effects on the gas flow inside the channels, in the primary flow direction (the main gas flow along the channels) by blocking the channels, and on the cross-sections by generating various secondary flows, as shown in Fig. 6(c)–(h).

3.2.2. Dean vortex evolution

For the *X–Z* plane at *Y* = 0.019 m, i.e., the plane cut near the entrance-turning-area shown in Fig. 6(a)–(h), it can be noticed that there are Dean vortices in the parallel channels. The lower vortex of the vortices gradually shrinks as the liquid water emerges from the porous layer into the channels. From the first to the last channels, the strength of the vortices increases because the maldistribution of the gas flow among the parallel channels increases; this phenomenon will be discussed in the later section titled "Mechanism of first and last channel phenomena".

For the *X–Z* plane at *Y* = 0.012 m, i.e., the plane cut in the middle of the domain in the *Y*-direction, there are distorted Dean vortices in the last channel. The lower vortex also gradually shrinks as the liquid water emerges from the porous layer into the channel. At a certain time (Fig. 6(h)), the lower vortex disappears completely, which shows the effects of gas–liquid interactions. There are no (distorted) Dean vortices from parallel channel #1 to #6 because these areas are removed from the influence of the Dean vortices around the entrance-turning-areas.

For the *X–Z* plane at *Y* = 0.005 m, i.e., the plane cut near the exit-turning-area, there are no Dean vortices because this plane is too far away from the entrance-turning-area.

3.3. General liquid water removal process in gas flow channels

The liquid water removal process in gas flow channels can be explained by Fig. 7. The *X–Y* view of the VOF of the liquid water inside the channels is shown in Fig. 7(a-1)–(n-1), and the water distributions in the three selected cross-sections with *Y* = 0.005 m, *Y* = 0.012 m and *Y* = 0.019 m are defined in Fig. 7(a-1) and shown in

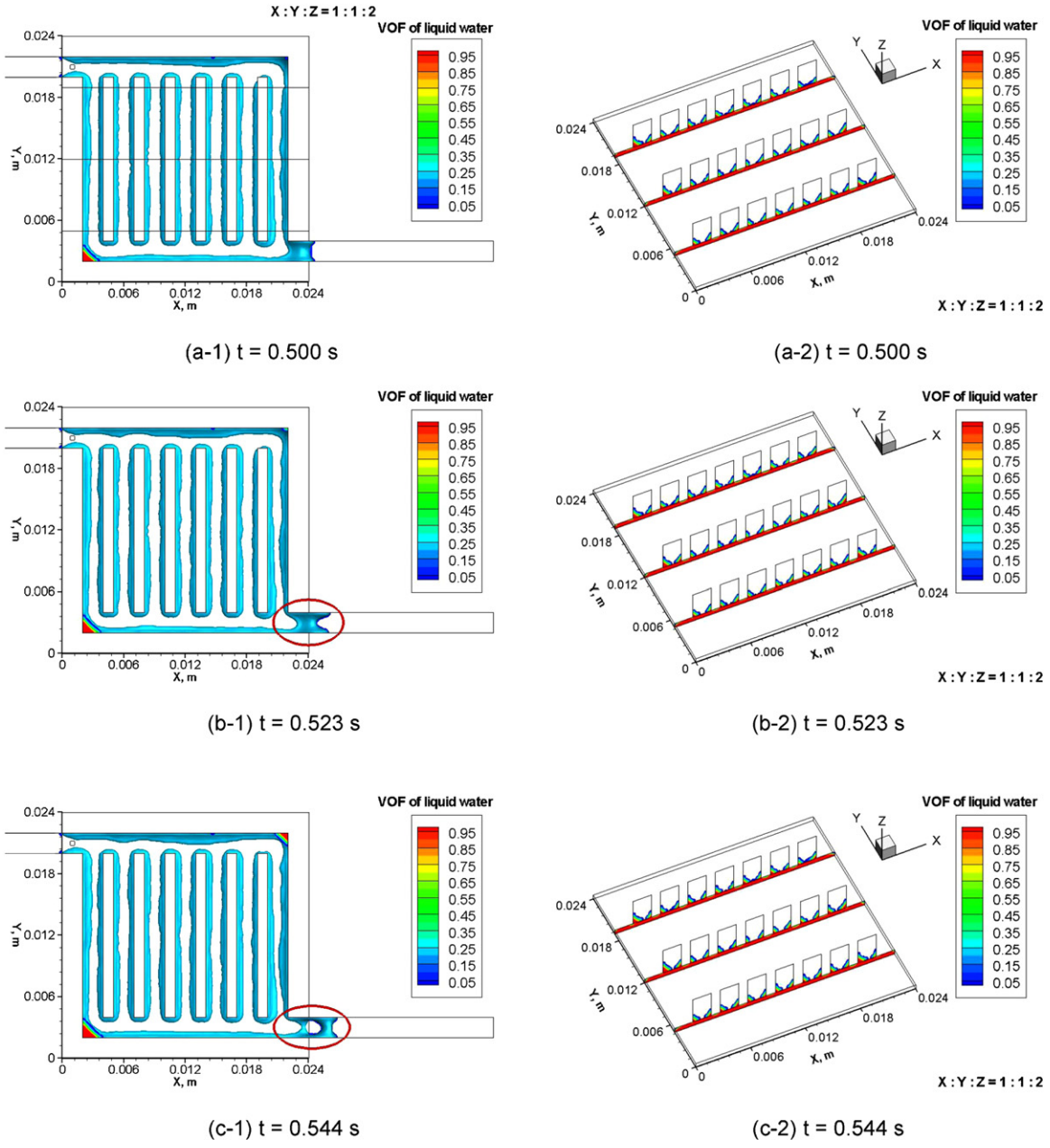

Fig. 7. (a–n) General process of liquid water removal in channels: (a-1) *t* = 0.500 s, (a-2) *t* = 0.500 s; (b-1) *t* = 0.523 s, (b-2) *t* = 0.523 s; (c-1) *t* = 0.544 s, (c-2) *t* = 0.544 s; (d-1) *t* = 0.546 s, (d-2) *t* = 0.546 s; (e-1) *t* = 0.555 s, (e-2) *t* = 0.555 s; (f-1) *t* = 0.590 s, (f-2) *t* = 0.590 s; (g-1) *t* = 0.655 s, (g-2) *t* = 0.655 s; (h-1) *t* = 0.724 s, (h-2) *t* = 0.724 s; (i-1) *t* = 0.759 s, (i-2) *t* = 0.759 s; (j-1) *t* = 0.920 s, (j-2) *t* = 0.920 s; (k-1) *t* = 0.965 s, (k-2) *t* = 0.965 s; (l-1) *t* = 0.994 s, (l-2) *t* = 0.994 s; (m-1) *t* = 1.171 s, (m-2) *t* = 1.171 s; (n-1) *t* = 1.300 s, (n-2) *t* = 1.300 s.

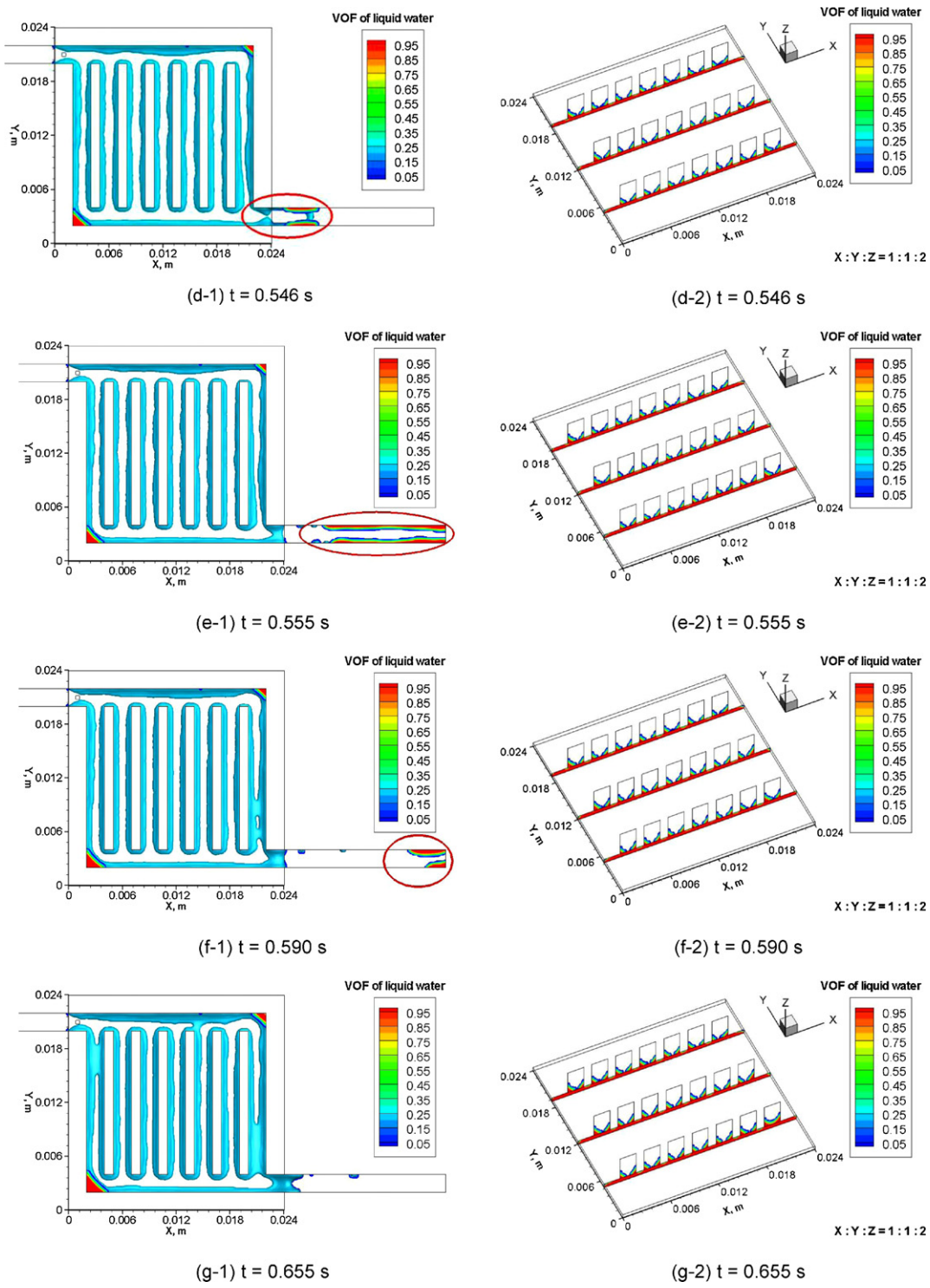

Fig. 7. (*Continued*)

the right column of Fig. 7(a-2)–(n-2); this information will help the reader understand the status of the liquid water blockage across parallel channels.

The liquid water coming from the porous layer near the peripheral zones of the four frames and the lands shown in Fig. 7(a) gradually develops into two liquid water streams, with the first stream accumulating at the bottom of the outlet manifold and the second stream accumulating on the side wall of the last parallel channel (#7). These two streams meet near the outlet joint (Fig. 7(a)) and gradually form a wheel shaft shape (two wheels connected by one shaft in the middle) (Fig. 7(b)). This shape is formed due to the combined effects of wall adhesion and liquid water surface tension. At the same time, the air streams from all directions also meet and merge into one stream at the outlet joint; this combined air stream continuously strikes the left side of the wheel shaft, forcing the wheel shaft to move along the outlet channel and break into a pair of wheel shafts (Fig. 7(c) and (d)). Then, this wheel shaft shape deforms into a top–bottom stratified flow pat-

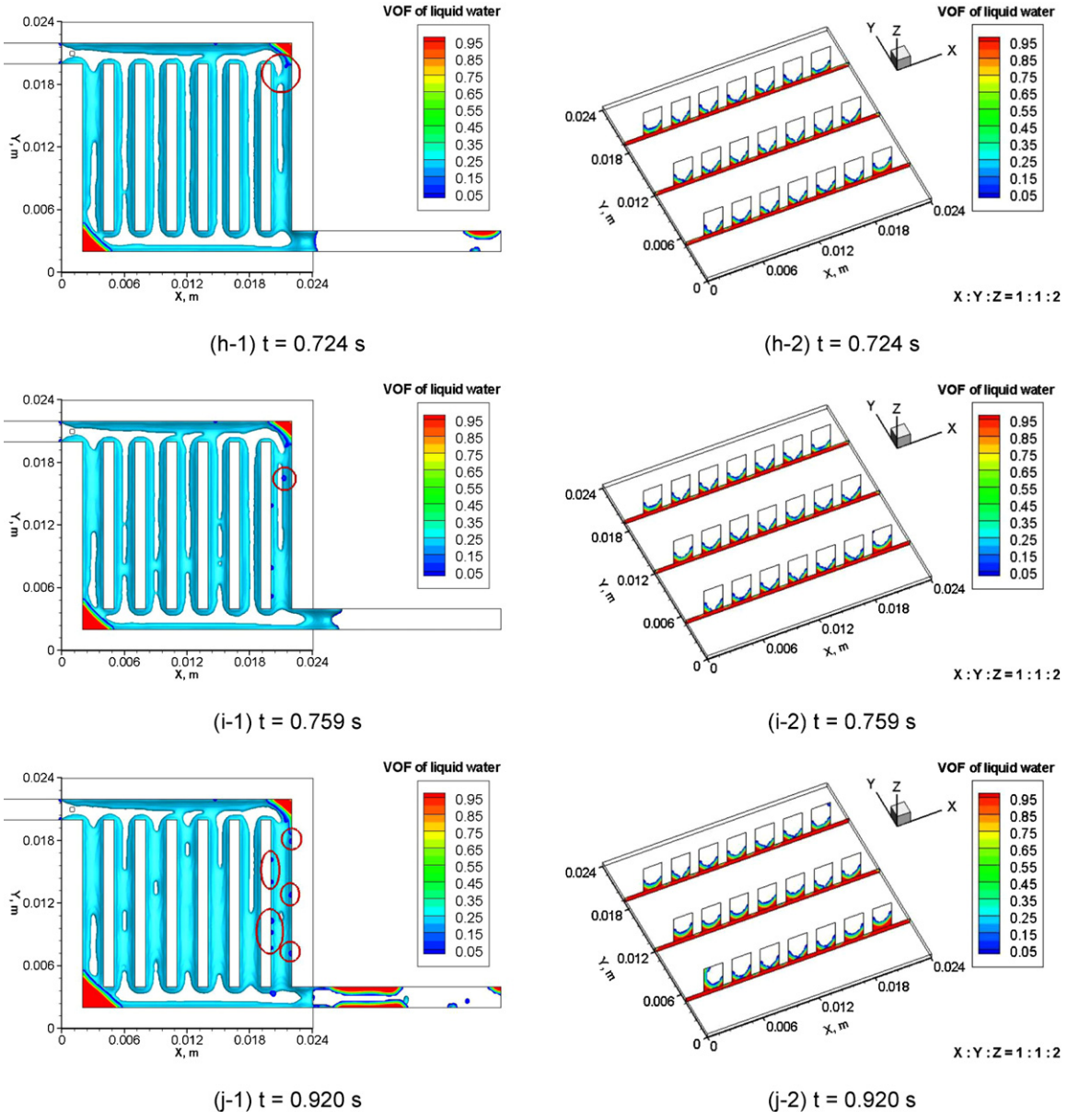

Fig. 7. (*Continued*)

tern while moving along the outlet channel to drain (Fig. 7(e) and (f)). These processes repeat for a period of time (Fig. 7(g)–(m)), and the liquid water eventually moves along the outlet channel with a top-stratified pattern (Fig. 7(n)). Within this time period, two interesting phenomena occur; i.e., the first and the last parallel channel phenomena. These phenomena will be explained in the following section.

3.3.1. *First and last parallel channel phenomena*

At a certain time instant (t = 0.590 s for the present case) and near the exit-turning-area (defined in Fig. 2) of the last parallel channel, the liquid water streams coming from the peripheral edge of the land and the edge of the right frame merge together (Fig. 7(f)). Then, as shown in Fig. 7(g), a similar merging process happens near the entrance-turning-area (defined in Fig. 2) of the first parallel channel due to the vortex that is caused by the inertia of the inlet air flow (Fig. 8(a)).

Almost immediately after the blockage of the first parallel channel occurs near the entrance-turning-area, liquid water starts to accumulate around the left-bottom corner of the outlet manifold. At the moment when this water front touches the left-bottom corner of the first land, the first parallel channel is blocked from the bottom (Fig. 8(b)). Then, this liquid water front continuously expands along the first channel from the bottom up (Fig. 7(k)–(n)) due to the lower pressure zone caused by the blockage near the first entrance-turning-area that is established just above the water front inside the first channel.

Around the time instant t = 0.724 s (Figs. 7(h) and 9(a)) at the entrance-turning-area of the last parallel channel, the liquid water stream coming from the peripheral edge of the land and the stream emerging from the edge of the right frame merge together. Almost immediately after this merge, the accumulated water in the right-top corner of channels starts to splash into small droplets as it is struck by the gas flow from the inlet manifold (Fig. 7(h)–(k)). There is a low pressure zone around the entrance-turning-area of the last parallel channel, which attracts droplets of liquid water from around the corner into the main flow stream. These small droplets continue to move toward the land wall and adhere to it due to

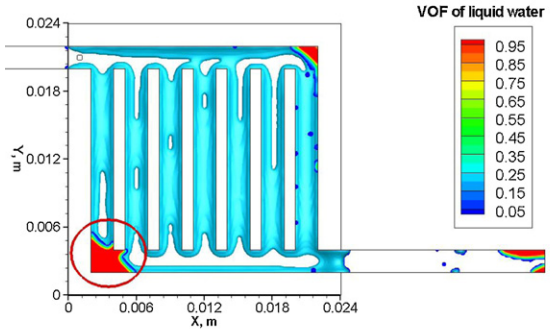

(k-1) t = 0.965 s

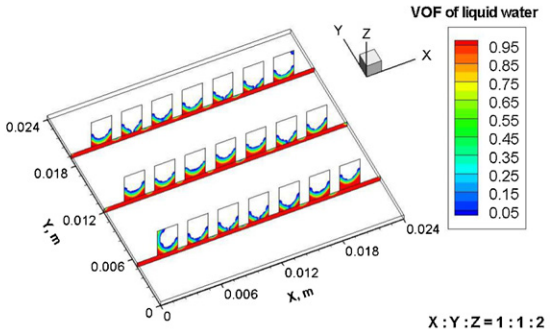

(k-2) t = 0.965 s

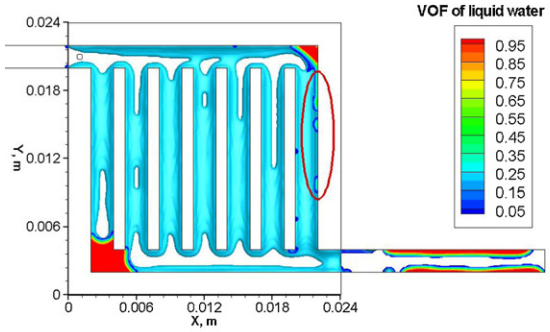

(l-1) t = 0.994 s

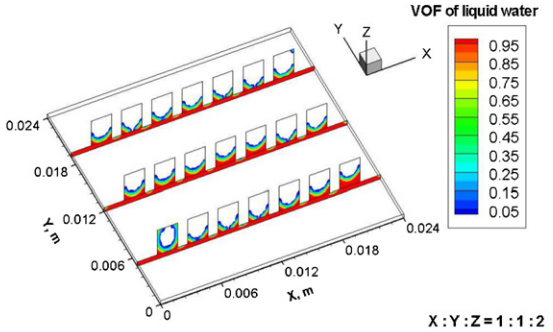

(l-2) t = 0.994 s

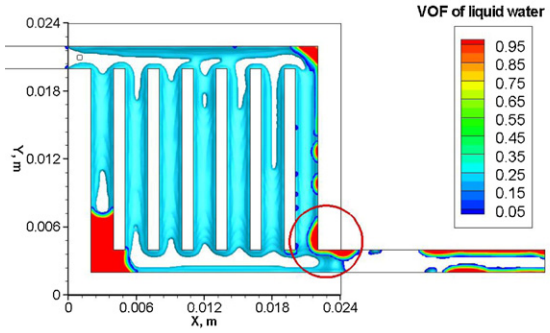

(m-1) t = 1.171 s

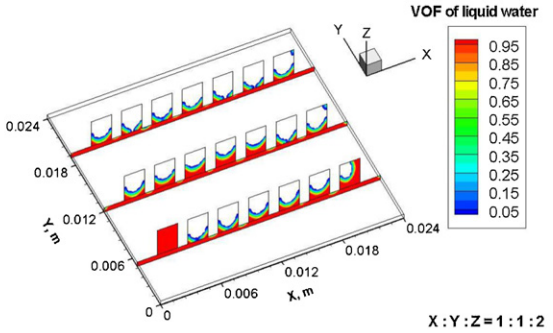

(m-2) t = 1.171 s

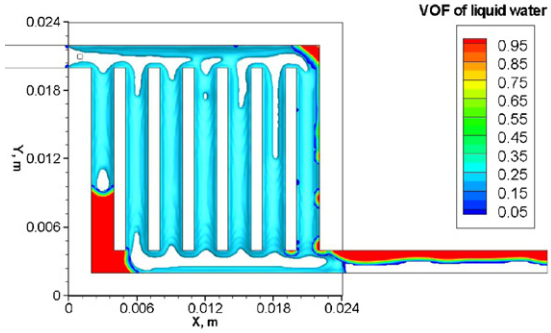

(n-1) t = 1.300 s

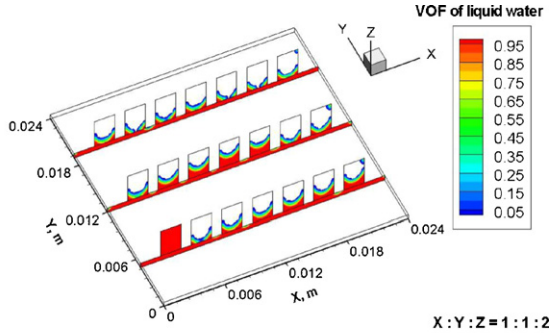

(n-2) t = 1.300 s

Fig. 7. (*Continued*).

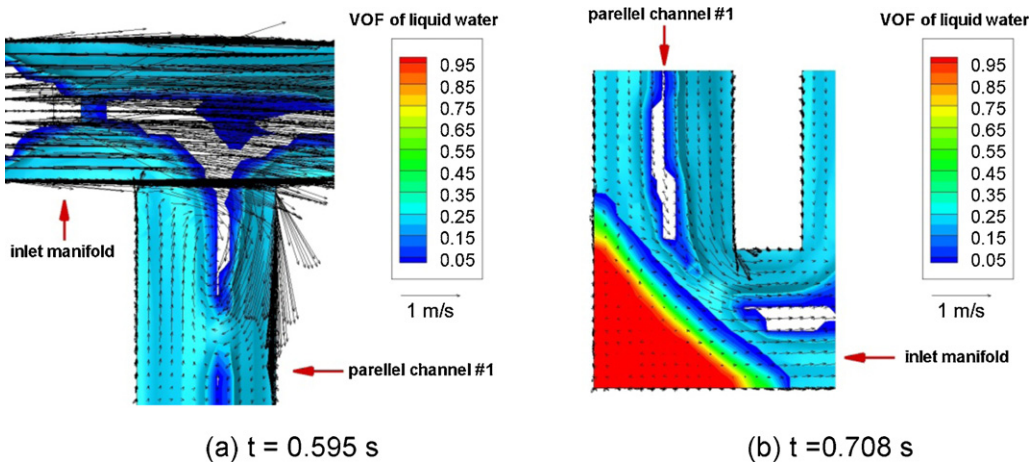

Fig. 8. (a) Enlarged view of liquid water emerging together around the entrance-turning-area of the first channel and (b) enlarged view of liquid water starts to block the left-bottom corner of channels. (a) $t = 0.595$ s and (b) $t = 0.708$ s.

the wall adhesion effect. The interaction between the airflow and the liquid water in the vicinity of corners can provide strong shear stress and can fragment some of the liquid water on the gas–liquid water interface into small droplets. These small droplets flow along the side wall of the right frame due to inertial forces and wall adhesion, and then, the small liquid water droplets merge into large droplets (Figs. 7(l) and 9(b)) that continuously flow along the side wall of the right frame, reaching the corner near the outlet joint and accumulating there. This accumulation is because that near the joint the surface tension forces and wall adhesion forces are large due to the large curvature of the wall.

Around time $t = 1.171$ s, as shown in Fig. 7(m), the liquid water that is accumulating around the corner of the right frame starts to drain out along the top side wall of the outlet channel. This type of flow is known as top-stratified drainage flow, and this effect becomes dominant after this point in time.

3.3.2. *Mechanism of first and last channel phenomena*

Fig. 9 shows the VOF and velocity distribution on three planes ($Y = 0.005$ m, $Y = 0.012$ m and $Y = 0.019$ m). At $t = 0.200$ s (Fig. 10(a)), when all liquid water still remains in the porous layer, the air distribution among parallel channels increases with increasing distance from the inlet joint (defined in Fig. 2), with the last channel having the maximum flowrate and velocity and the first channel having the minimum flowrate and velocity. Fundamentally, this maldistribution of gas flow is caused by the parallel channel design; this point is also discovered by Wang et al. in his recent publication [28]. The maldistribution of reactant gas (air) flow then creates a maldistribution of liquid water in the parallel channels and porous layers. The maldistribution of liquid water, in return, further affects the of the reactant gas flow (Fig. 10(b)). This emphasizes that liquid water management is still one of the critical challenges for PEMFC designs.

3.4. *Porosity effect on drainage performance*

To investigate the influence of the porosity of the porous layer on the water flooding process, three cases with different porosities (0.3, 0.5 and 0.8) were studied. The general liquid water flooding processes are quite similar among these three cases, whereas the drainage performance parameters, such as the water emerging time (the instant when the liquid water from the porous layer emerges into the gas flow channels) and the water departure time (the instant when the liquid water begins to depart from the outlet of the fuel cell), are different. The water emerging time, departure time and porosity for these three cases are shown in Fig. 11. The results reveal that both times change in and approximately linear fashion with respect to porosity, i.e., larger porosities give longer times because the porous layer with larger porosity can accommodate more liquid water for a longer time.

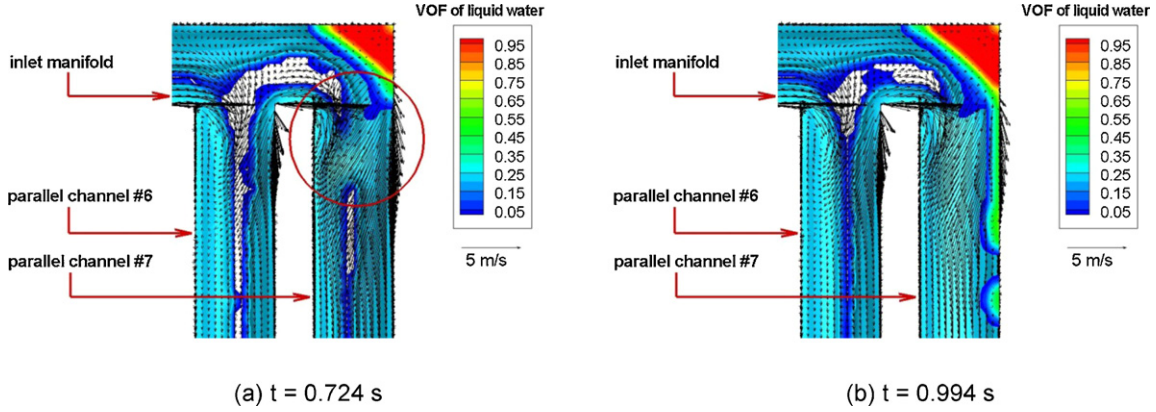

Fig. 9. (a, b) Enlarged view of liquid water splashing phenomenon at right-top corner of channels: (a) $t = 0.724$ s and (b) $t = 0.994$ s.

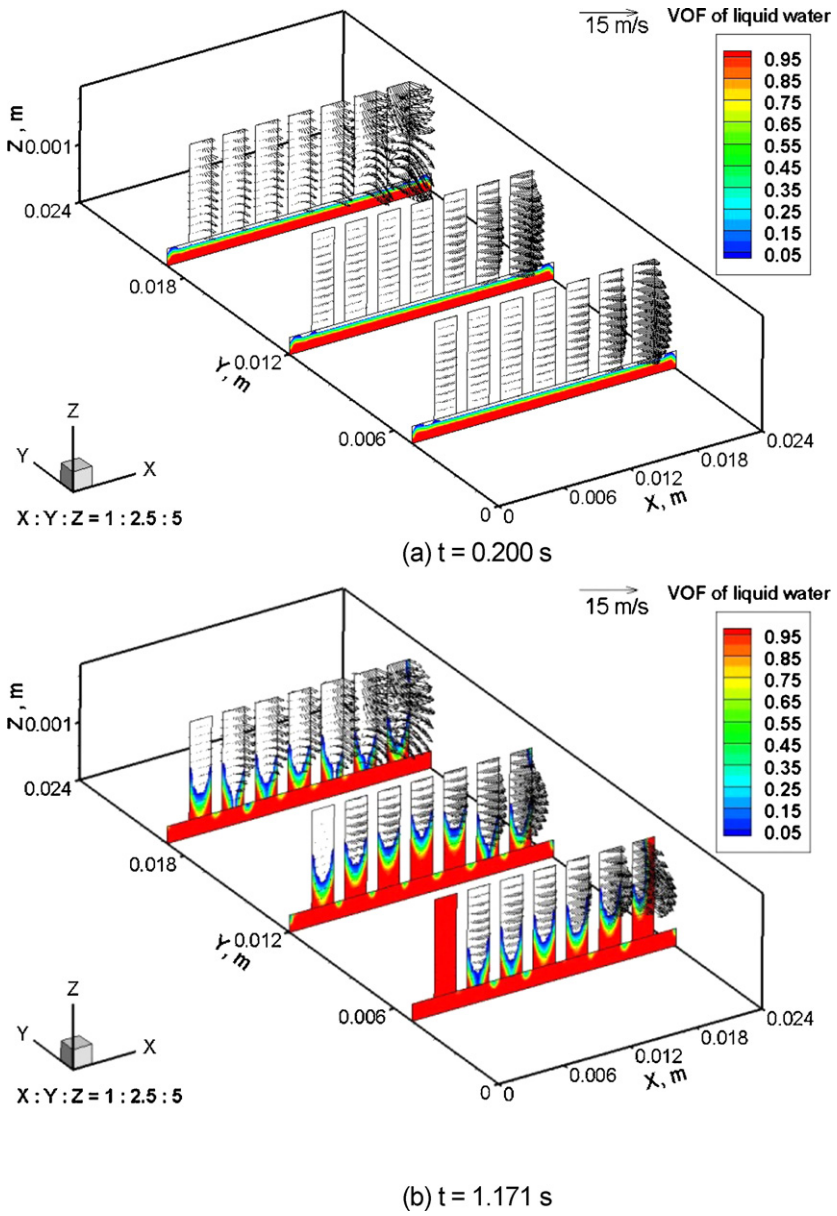

Fig. 10. (a, b) VOF and velocity distribution on three planes (Y = 0.005 m, Y = 0.012 m and Y = 0.019 m): (a) t = 0.200 s and (b) t = 1.171 s.

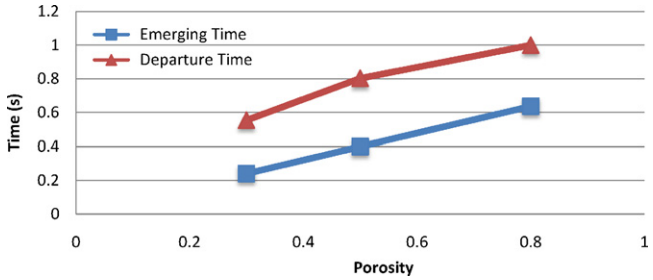

Fig. 11. Porosity affection on drainage performance.

4. Conclusions

The liquid water flooding process in the porous layer and in the parallel channels on the cathode side of a PEMFC was investigated by conducting a three-dimensional, unsteady two-phase flow using a VOF model in FLUENT®. The porosity effect on the liquid water draining process was also studied. The main conclusions can be summarized as follows:

(1) Liquid water flooding behavior in the cathode is directly influenced by the parallel channel design.
(2) The liquid water accumulation usually starts from the zones under the frames inside the porous layer.
(3) The liquid water from the porous layer first enters into the air flow channels through the edges of lands and frames.
(4) There are two important phenomena (the first channel phenomenon and last channel phenomenon) that significantly affect the liquid–water flow patterns in the outlet channel.
(5) The porosity of the porous layer is one of the important factors which affect the water removal process. The porosity can change the drainage performance by changing the time for liquid water to enter into and drain out of the channels.

In the future, the liquid water flooding processes for cathodes with different channel designs will be investigated and compared

to this parallel channel study. This comparison will aid in gaining a fundamental understanding of the effects of channel design on the liquid water removal process.

Acknowledgements

The authors are grateful for the support given by the AUTO21^{TM}, the Network of Centers of Excellence (Grant D303-DFC), the Natural Sciences and Engineering Research Council of Canada (NSERC), and the University of Windsor.

References

[1] X. Li, I. Sabir, Review of bipolar plates in PEM fuel cells: flow-field designs, International Journal of Hydrogen Energy 30 (2005) 359–371.
[2] R. O'Hayre, S.-W. Cha, W. Colella, F.B. Prinz, Fuel Cell Fundamentals, John Wiley & Sons, Inc., 2006, pp. 163–166.
[3] K. Jiao, X. Li, Water transport in polymer electrolyte membrane fuel cells, Progress in Energy and Combustion Science (2010), doi:10.1016/j.pecs.2010.06.002.
[4] D. Singh, D.M. Lu, N. Djilali, A two-dimensional analysis of mass transport in proton exchange membrane fuel cells, International Journal of Engineering Science 37 (1999) 431–445.
[5] N. Djilali, D. Lu, Influence of heat transfer on gas and water transport in fuel cells, International Journal of Thermal Sciences 41 (2002) 29–40.
[6] S. Dutta, S. Shimpalee, J.W. Van Zee, Three-dimensional numerical simulation of straight channel PEM fuel cells, Journal of Applied Electrochemistry 30 (2000) 135–146.
[7] S.W. Cha, R. O'Hayre, Y. Saito, F.B. Prinz, The scaling behavior of flow patterns: a model investigation, Journal of Power Sources 134 (2004) 57–71.
[8] A.A. Kulikovsky, Numerical simulation of a new operational regime for a polymer electrolyte fuel cell, Electrochemistry Communications 3 (2001) 460–466.
[9] J.S. Yi, J.D. Yang, C. King, Water management along the flow channels of PEM fuel cells, Journal of AIChE 50 (2004) 2594–2603.
[10] L. You, H. Liu, A two-phase flow and transport model for the cathode of PEM fuel cells, International Journal of Heat Mass Transfer 45 (2002) 2277–2287.
[11] Z.H. Wang, C.Y. Wang, K.S. Chen, Two-phase flow and transport in the air cathode of proton exchange membrane fuel cells, Journal of Power Sources 94 (2001) 40–50.
[12] M.M. Mench, Q.L. Dong, C.Y. Wang, In situ water distribution measurements in a polymer electrolyte fuel cell, Journal of Power Sources 124 (2003) 90–98.
[13] J.E. Dawes, N.S. Hanspal, O.A. Family, A. Turan, Three-dimensional CFD modelling of PEM fuel cells: an investigation into the effects of water flooding, Journal of Chemical Engineering Science 64 (2009) 2781–2794.
[14] G. Luo, Y. Ji, C.-Y. Wang, P.K. Sinha, Modeling liquid water transport in gas diffusion layers by topologically equivalent pore network, Electrochimica Acta 55 (2010) 5332–5341.
[15] P. Quan, B. Zhou, A. Sobiesiak, Z. Liu, Water behavior in serpentine microchannel for proton exchange membrane fuel cell cathode, Journal of Power Sources 152 (2005) 131–145.
[16] K. Jiao, B. Zhou, P. Quan, Liquid water transport in parallel serpentine channels with manifolds on cathode side of a PEM fuel cell stack, Journal of Power Sources 154 (2006) 124–137.
[17] K. Jiao, B. Zhou, P. Quan, Liquid water transport in straight micro-parallel-channels with manifolds for PEM fuel cell cathode, Journal of Power Sources 157 (2006) 226–243.
[18] K. Jiao, B. Zhou, Innovative gas diffusion layers and their water removal characteristics in PEM fuel cell cathode, Journal of Power Sources 169 (2007) 296–314.
[19] K. Jiao, B. Zhou, Effects of electrode wettabilities on liquid water behaviours in PEM fuel cell cathode, Journal of Power Sources 175 (2008) 106–119.
[20] K. Jiao, B. Zhou, Accelerated numerical test of liquid behavior across gas diffusion layer in proton exchange membrane fuel cell cathode, Journal of Fuel Cell Science and Technology 5 (November) (2008) 041011.
[21] X. Zhu, P.C. Sui, N. Djilali, Dynamic behaviour of liquid water emerging from a GDL pore into a PEMFC gas flow channel, Journal of Power Sources 172 (2007) 287–295.
[22] A.D. Le, B. Zhou, A general model of proton exchange membrane fuel cell, Journal of Power Sources 182 (2008) 197–222.
[23] A.D. Le, B. Zhou, Fundamental understanding of liquid water effects on the performance of a PEMFC with serpentine-parallel channels, Electrochimica Acta 54 (2009) 2137–2154.
[24] A.D. Le, B. Zhou, A numerical investigation on multi-phase transport phenomena in a proton exchange membrane fuel cell stack, Journal of Power Sources 195 (2010) 5278–5291.
[25] A.D. Le, B. Zhou, H.-R. Shiu, C.-I. Lee, W.-C. Chang, Numerical simulation and experimental validation of liquid water behaviors in a proton exchange membrane fuel cell cathode with serpentine channels, Journal of Power Sources 195 (2010) 7302–7315.
[26] Fluent 6.3 Manual, Fluent Inc., 2006.
[27] D.B. Kothe, W.J. Rider, S.J. Mosso, J.S. Brock, Volume tracking of interfaces having surface tension in two and three dimensions, AIAA, 1996, 96-0859.
[28] S. Basu, C.-Y. Wang, K.S. Chen, Analytical model of flow maldistribution in polymer electrolyte fuel cell channels, Chemical Engineering Science (2010), doi:10.1016/j.ces.2010.08.036.